

Enhancement of the quantum dot fluorescence intensity by Au nanoparticle decoration of a porous silicon photonic crystal

Lei He¹ · Zhenhong Jia² · Jun Zhou³ · Hongyan Zhang¹ · Xiaoyi Lv² · Difei Sun¹

Received: 22 March 2016 / Accepted: 6 April 2017 / Published online: 21 April 2017
© Springer-Verlag Berlin Heidelberg 2017

Abstract A new way to enhance the photoluminescence of CdSe/ZnS quantum dots embedded in porous silicon (PSi) is reported, which results in the double enhancement of the quantum dot (QD) fluorescence due to Au nanoparticle decoration and the porous silicon having a distributed Bragg reflector (DBR) structure. Through the dropwise addition of a solution of CdSe/ZnS QDs on Au nanoparticle-decorated porous silicon samples, the QDs successfully infiltrated the porous silicon substrate. Among the fluorescence intensities of QDs/single-layer PSi, QDs/multilayer PSi, QDs/Au/single-layer PSi and QDs/Au/multilayer PSi, we find that the fluorescence of the QD-infiltrated multilayer PSi is stronger than that of the single-layer sample, and the multilayer sample decorated with Au nanoparticles shows further improvement of the fluorescence intensity through plasmonic effects. PSi, as a substrate with a spongy structure, offers favorable conditions for enhancing fluorescence intensity.

1 Introduction

Quantum dots (QDs) are zero-dimensional materials that exhibit highly desirable photoluminescence and optoelectronic properties, including high quantum yield, resistance

to photobleaching, broad excitation spectra, tunability of nanoscale size and structure, fluorescence that spans the UV–Vis–NIR spectrum, and bioconjugation capabilities [1]. In recent years, QDs have been applied in the biomedical field because of their important fluorescence properties and good biocompatibility. For example, QDs have been used as fluorescent tags in biomarkers, immunoassays, guided drug delivery, cellular imaging, and fluorescence resonance energy transfer (FRET)-based sensors [2–7]. Au nanoparticles (NPs) have been applied in optoelectronic devices because of their surface plasmon resonance (SPR); moreover, Au NPs are capable of biological conjunction, and thus have been widely applied for molecular biological detection [8–11]. Porous silicon (PSi) is of great interest in biosensing because of its large internal surface area, good biocompatibility, and ease of functionalization [12–14]. Moreover, PSi can be easily made into photonic devices with different structures. Combining QDs with PSi can lead to the fabrication of biosensors with high sensitivity and excellent performance. Shi et al. enhanced the fluorescence of R6G by Au NP deposition on PSi Bragg reflectors [15]. Gaur et al. [16] embedded QDs inside a PSi microcavity and detected biotin in streptavidin-functionalized PSi biosensors (the biotin detection limit was 0.5 fg/mm²). Au NPs can enhance the luminescence of QDs through localized surface plasmon (LSP) resonance [17, 18]; however, improving the photoluminescence properties of QDs by Au NP deposition in PSi photonic crystals has not been reported.

In this work, we infiltrated QDs into Au NP-decorated PSi and enhanced the fluorescence of the QDs through LSP [19] resonance of the Au NPs. In addition, we gained further improvement of the fluorescence properties of QDs using a photonic crystal device with Bragg structures. This QD/Au/PSi optical device has potential applications in biological detection.

✉ Zhenhong Jia
jzhh@xju.edu.cn

¹ School of Physical Science and Technology, Xinjiang University, Urumqi 830046, People's Republic of China

² School of Information Science and Engineering, Xinjiang University, Urumqi 830046, People's Republic of China

³ Department of Physics, Ningbo University, Ningbo 315211, People's Republic of China

2 Materials and methods

2.1 CdSe/ZnS quantum dots

QDs were purchased from Wuhan Jiayuan Quantum Dots Co. Ltd. (Wuhan, China). As shown in Fig. 1, the sizes of the graphene oxide QDs range from 7.5 to 8.5 nm, and the fluorescence peak is located at 620 nm at an excitation wavelength of 380 nm.

2.2 PSi device fabrication

The PSi substrate was fabricated using p-type Si(100) with a resistivity of 0.03–0.06 $\Omega \text{ cm}^{-1}$ by electrochemical etching in electrolyte (HF:CH₃CH₂OH 1:1 in volume). Before electrochemical anodization, all of the pieces were cleaned successively with solutions of carbinol, alcohol, and deionized water. The electrochemical etching parameters were manipulated to obtain samples of periodically changing porosity or refractive index. The PSi Bragg reflector has a bandgap area and high reflectivity. PSi Bragg reflectors with different bandgap centers were prepared by controlling the electrochemical etching time and electric current density according to Eq. 1:

$$m\lambda_{\text{Bragg}} = 2(n_L d_L + n_H d_H) \quad (1)$$

where m is an integer, n_L (n_H) and d_L (d_H) are the low (high) refractive index and thickness of the PSi layers, respectively, and λ_{Bragg} is the center of the bandgap. The refractive index was tested using an automatic elliptic polarization apparatus (SC620); the results indicated that the refractive indices of multilayer PSi are 1.21 (n_L) and 1.78 (n_H). A multilayer PSi device with a bandgap center at 605 nm was produced, as the bandgaps of the samples red-shift after oxidation, silanization, and Au NP infiltration. The bandgap area should overlap with the fluorescence emission peak of the QDs after infiltration.

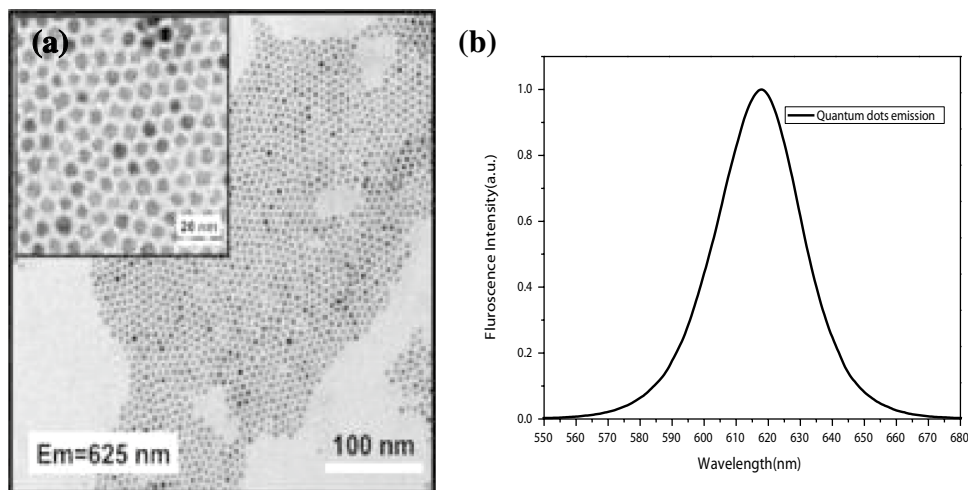
The multilayer samples consisted of two parts: a single-layer section and a distributed Bragg reflector (DBR) multilayer section. The single-layer PSi was fabricated using a current density of 105 mA/cm² for 4 s, while the 12 periodic DBR structures were fabricated using an alternating current density of $I_H = 100 \text{ mA cm}^{-2}$ and $I_L = 20 \text{ mA cm}^{-2}$. The etching times for each layer were 1.6 and 2.2 s, respectively. For a reasonable comparison, the single-layer sample was single-layer PSi. The etching conditions of this sample were identical to those in the first part of the multilayer sample. As illustrated in Fig. 2, the average diameter of the PSi pores is approximately 30 nm, and the diameter of the Au NPs is approximately 8 nm. A 3:1 ratio of pore to Au NP size was the minimum required for attachment of the spherical infiltrated species [20] so that the pore size permits Au NP infiltration. Figure 3 shows a cross-sectional SEM image of the PSi Bragg reflector. The dark colored PSi layers were formed by etching with a current density of 100 mA cm⁻², and the light-colored layers were etched with a current of 20 mA cm⁻².

After being etched, the substrates were cleaned with deionized water and air dried at room temperature. Then, all of the samples were oxidized in hydrogen peroxide (30%) at 80 °C for 3 h. Then, the oxidized PSi samples were immersed in a 5% solution of APTES in a water/methanol mixture (v/v, 1:1) for 45 min at room temperature to successfully attach the QDs and Au NPs to the PSi wall. After the reaction time was complete, the sample was washed in toluene to remove any unreacted APTES molecules. The sample was then baked at 100 °C for 10 min.

2.3 The preparation of Au NPs

We prepared Au NPs following a method reported in the literature [21, 22]. A total of 2 ml of an aqueous solution of HAuCl₄ (0.1 mM) was added to 100 ml of water and heated

Fig. 1 **a** SEM image of the QDs used in our work. **b** Photoluminescence spectra of the QDs at an excitation wavelength of 380 nm



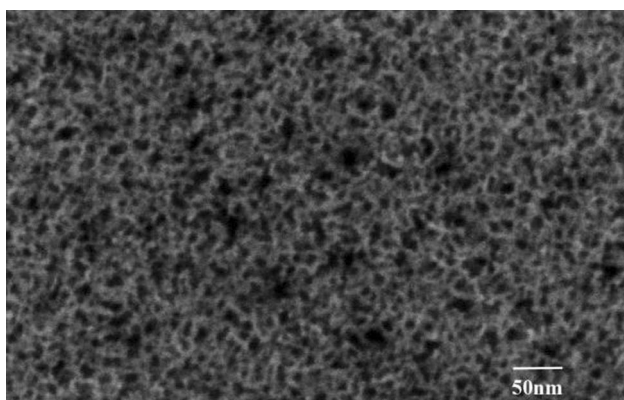


Fig. 2 Top-view SEM image of multilayer PSi

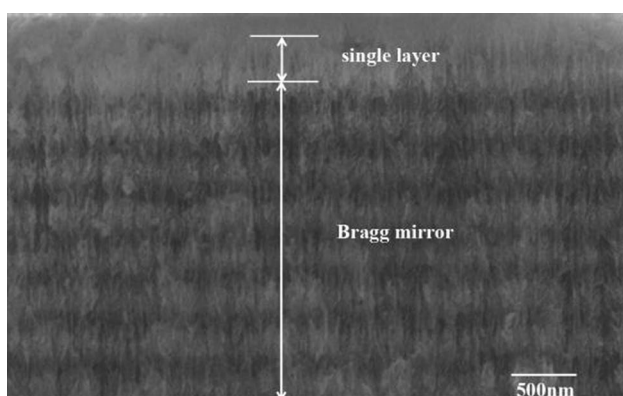


Fig. 3 Cross-sectional SEM image of multilayer PSi

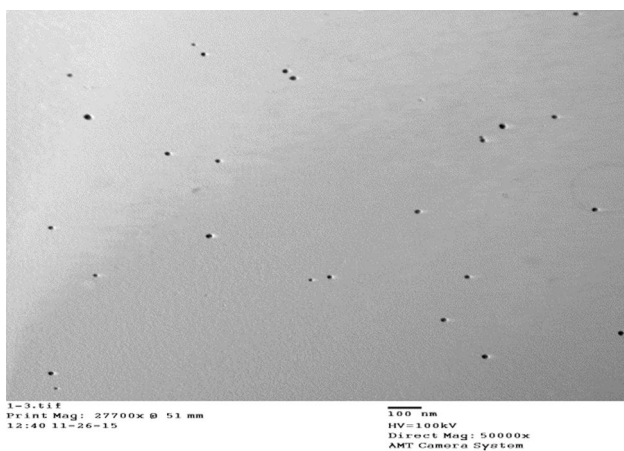


Fig. 4 TEM image of the Au NPs

to boiling; then, 4 ml of trisodium citrate (1.1 mM) solution was quickly added. After 10 min, the solution was left undisturbed for 1 h at room temperature. The prepared Au NPs are shown in Fig. 4.

2.4 Gold NPs deposited on PSi

The silanized PSi samples were immersed in the colloidal Au NP solution for 8 h, and the AuNPs slowly aggregated onto the PSi [15]. Then, the PSi samples were rinsed with deionized water and dried in air.

2.5 QDs infiltrated into PSi

A total of 4 μ l (0.4 μ mol/l) of QD solution was allowed to trickle over the silanized PSi samples for 6 h at room temperature. The QDs slowly aggregated onto the PSi. The binding of QDs to the PSi sample surface was achieved through the nitrogen lone pair of the APTES amine group [1]. The samples were then washed in deionized water to remove any redundant QDs on the surface. Finally, the PSi samples were allowed to air dry.

2.6 Spectral detection of sample

The reflection and photoluminescence were determined using a spectrophotometer (Hitachi U-4100, Japan) and fluorescence spectrophotometer (Hitachi F-4600, Japan), respectively. The excitation wavelength was 500 nm. The morphology of the PSi Bragg reflectors was detected by a ZEISS SUPRA55 VP scanning electronic microscope (SEM).

3 Results and discussion

The reflectance spectra after each step in the preparation of the multilayer PSi sample are shown in Fig. 5a–d. Figure 5a shows the reflectance spectra of pristine PSi and oxidized PSi. Upon oxidation, the reflectance spectrum blue-shifted owing to conversion of the high-index (~ 3.45) silicon regions into low-index (~ 1.5) SiO_2 . Figure 5c provides proof of the experimental infiltration of Au NPs into the pores, because Au NPs have inherently negative permittivities, and the reflectance spectra will blue-shift in the event Au NPs are infiltrated into the pores. As shown in Fig. 5d, the reflection spectrum of the PSi Bragg reflector red-shifted after the QDs were deposited, which indicates that while some QDs may be deposited on the surface of PSi, it is also likely that some QDs infiltrated into the pores. The noticeable red-shift in the reflectance spectra following QD deposition is indicative of QD infiltration and attachment to the PSi pore walls. This behavior results from the QDs depositing on the surface of PSi and increasing the effective refractive index. As shown in Fig. 6, the fluorescence intensity changed markedly after CdSe/ZnS QD infiltration, which further illustrates that QDs successfully infiltrated into PSi.

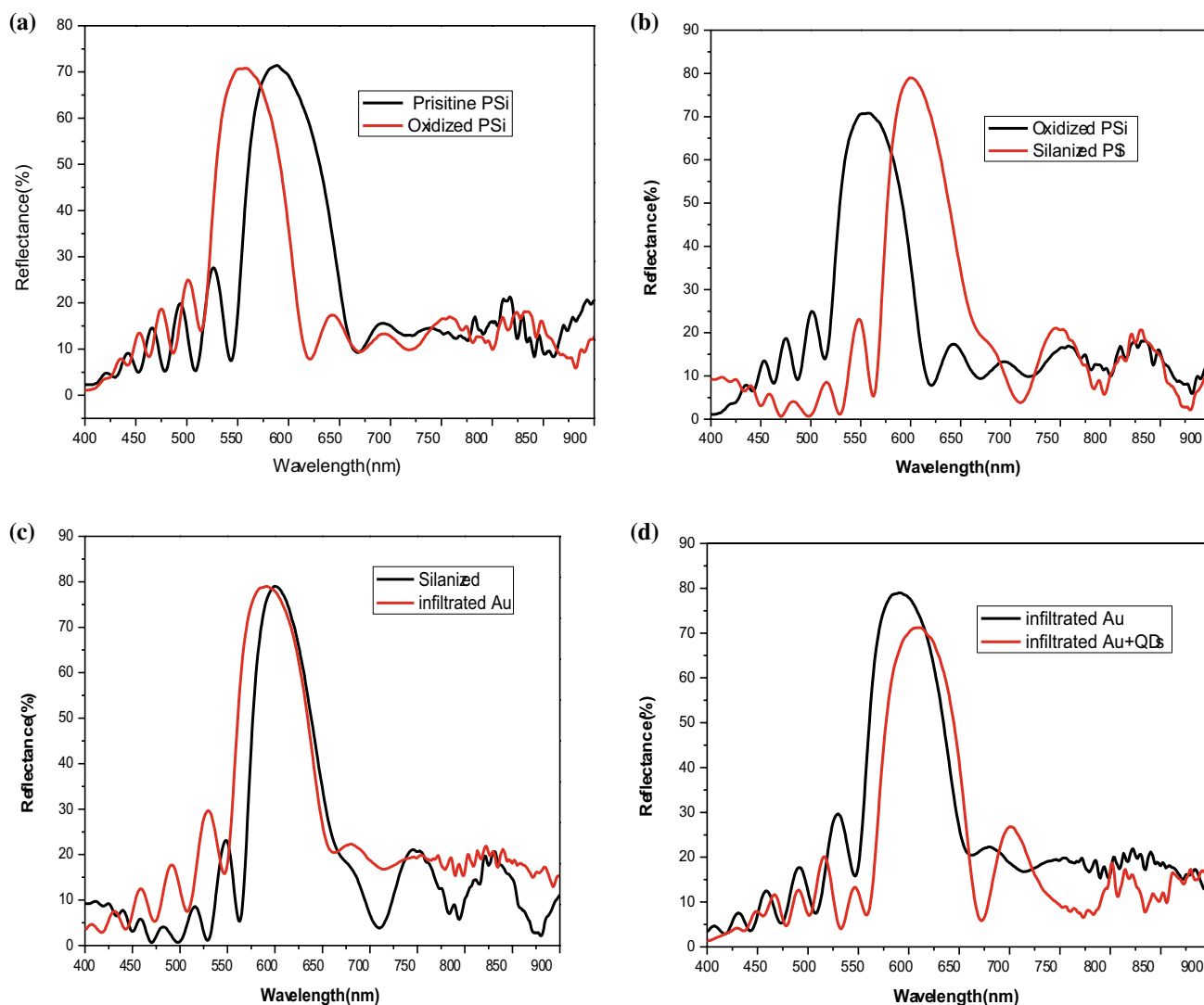


Fig. 5 Reflectance spectra after each step in the preparation of the multilayer PSi sample: **a** pristine PSi (black line) and oxidized PSi (red line); **b** oxidized PSi (black line) and silanized PSi (red line); **c**

silanized PSi (black line) and Au-infiltrated PSi (red line); and **d** Au-infiltrated PSi (black line) and Au- and QD-infiltrated PSi (red line)

Comparing the fluorescence spectrum of multilayer PSi with that of the single-layer sample (Fig. 7), an obvious enhancement in the fluorescence intensity of the multilayer sample can be seen. The excitation wavelength (500 nm) is located outside of the bandgap of multilayer PSi, causing the reflectivity coefficient to be lower, while the transmission coefficient of the excitation light inside the multilayer PSi was higher. Meanwhile, fluorescence in the QD emission spectrum was located at 625 nm, which is in the bandgap of multilayer PSi. Therefore, the structures prevented the upward and downward fluorescence from transmitting inside the PSi and reflected the light to the surface of the PSi, such that the fluorescence of the sample was enhanced.

The final reflectance spectra for the devices with and without Au NPs in the pores are provided in Fig. 8, and the two devices demonstrated similar reflectivities at QD emission wavelengths. Through comparison of the fluorescence intensity of the deposited PSi samples with or without Au NP decoration (as shown in Fig. 10), we can obtain clear evidence of the LSP-enhanced QD fluorescence intensity. We can conclude that Au NPs can effectively enhance the fluorescence intensity of CdSe/ZnS QDs infiltrated in PSi, which may be caused by the LSP resonance of the Au NPs. The LSP effect can be produced on nanostructured metals when incident light excites the sample. This excitation greatly intensifies the local electric field around the Au NPs, and the

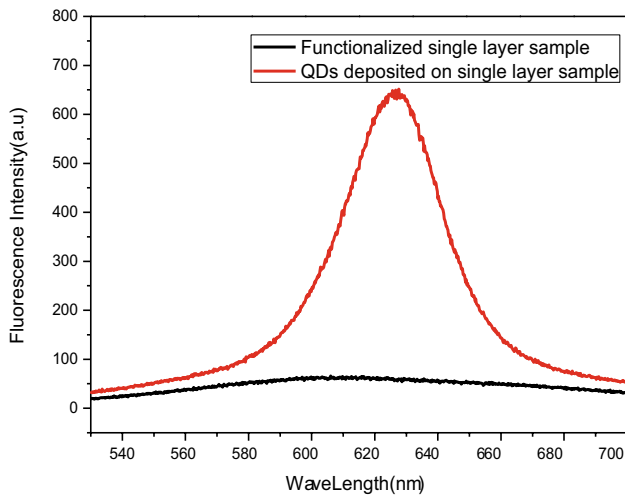


Fig. 6 Fluorescence intensity of the single-layer PSi sample with and without QD coupling

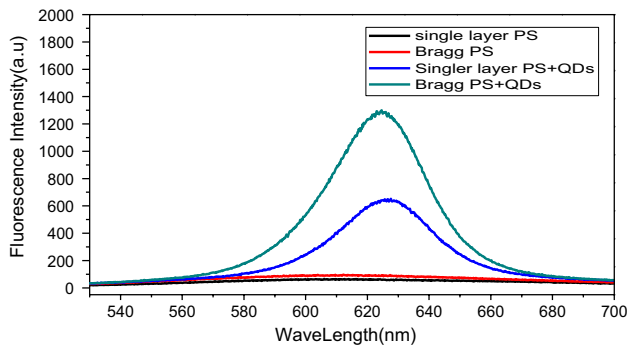
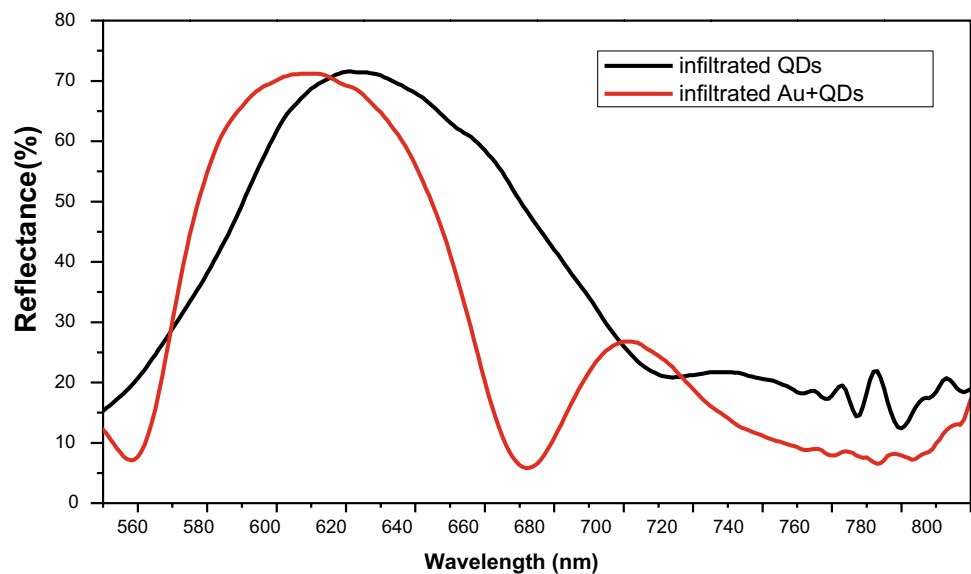


Fig. 7 Fluorescence emission spectra of the undeposited and deposited PSi samples: fluorescence of the single-layer sample (black line); fluorescence of the multilayer Bragg sample (red line); fluorescence of the deposited single-layer sample (blue line); fluorescence of the deposited Bragg sample, whose high reflectance band is located in the fluorescence region (green line)

Fig. 8 Final reflectance spectra for the devices (after QD infiltration) with (red line) and without (black line) Au NPs in the pores



excitation rate of the luminescent molecules is increased by the enhanced local electric field, enhancing the fluorescence signal. Certainly, the effect on the fluorescence is related to the distance between the metal NPs and the fluorescent material. Photoluminescence quenching occurs when metal nanostructures, such as Au NPs, are positioned within 2 nm of light-emitting materials. However, when the distance between the two nanosystems is in the range of 5–20 nm, the photoluminescence can be enhanced by SP coupling [17]. In our device, the distance between most of the Au NPs and QDs meets the requirement for fluorescence enhancement because of the porous structure of PSi. Moreover, the emission wavelength of CdSe/ZnS QDs is located at 620 nm, which is far from the absorption wavelength (520 nm) of Au NPs, and thus fluorescence quenching resulting from resonance energy transfer is not a dominant factor. In Fig. 9, we provide the absorption spectra of Au NPs and QDs.

4 Conclusion

We prepared one-dimensional PSi photonic crystals with a bandgap that covered the fluorescent emission peak of CdSe/ZnS QDs and decorated the PSi substrate with Au NPs. We then infiltrated CdSe/ZnS QDs into the PSi, which had a Bragg structure. The effect of the Au/multilayer PSi substrate on the QD fluorescence was studied. Comparing the fluorescence intensity of QDs/single-layer PSi, QDs/multilayer PSi, and QDs/Au/multilayer PSi, we conclude that the Au/multilayer PSi substrate effectively enhances the fluorescence intensity of the CdSe/ZnS QDs. Thus, double fluorescence enhancement can be realized by Au NP decoration of PSi with a DBR structure. This unique

Fig. 9 Absorption spectra of Au NPs and QDs

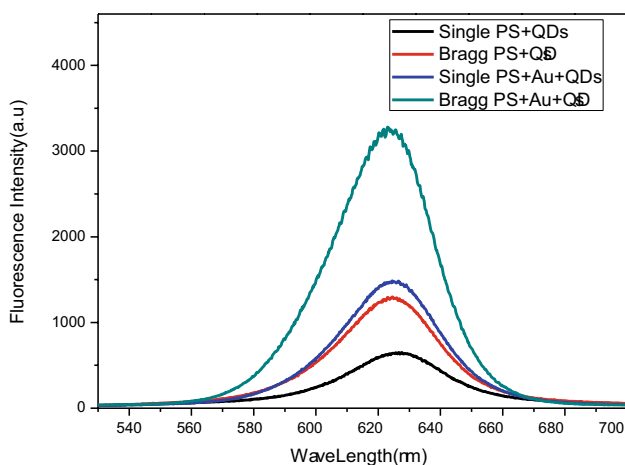
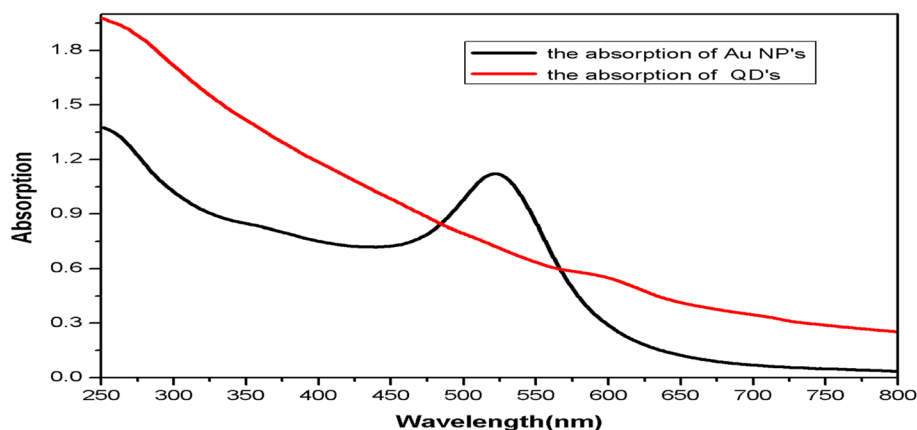


Fig. 10 Fluorescence spectrum of each sample: QD fluorescence on the single-layer PSi film (*black line*); QD fluorescence on the multilayer PSi film (*red line*); QD fluorescence in the Au NP-decorated single-layer PSi film (*blue line*); and QD fluorescence in the Au NP-decorated multilayer PSi film (*green line*)

substrate is expected to have potential applications as a new fluorescence biosensor with good biological compatibility and high sensitivity.

Acknowledgements This work was supported by the National Science Foundation of China (Nos. 61 575 168, 11504313 and 61665011) and the Xinjiang Science and Technology Project (No. 201412112).

References

- G. Gaur, D.S. Koktysh, S.M. Weiss, *Funct. Mater.* **23**, 3604–3614 (2013)
- B. Dubertret, P. Skourides, D.J. Norris, V. Noireaux, A.H. Brivanlou, A. Libchaber, *Science* **298**, 1759 (2002)
- M. Howarth, K. Takao, Y. Hayashi, A.Y. Ting, *Proc. Natl. Acad. Sci. USA* **102**, 7583 (2005)
- G. Rousserie, A. Sukhanova, K. Even-Desrumeaux, F. Fleury, P. Chames, D. Baty, V. Oleinikov, M. Pluot, J.H.M. Cohen, I. Nabiev, *Crit. Rev. Oncol. Hematol.* **74**, 1 (2010)
- M. Suzuki, Y. Husimi, H. Komatsu, K. Suzuki, K.T. Douglas, *J. Am. Chem. Soc.* **130**, 5720 (2008)
- I.L. Medintz, H. Mattoussi, A.R. Clapp, *Int. J. Nanomed.* **3**, 151 (2008)
- K. Sapsford, T. Pons, I. Medintz, H. Mattoussi, *Sensors* **6**(8), 925–953 (2006)
- L. Marques, F.U. Hernandez, S.W. James, S.P. Morgan, M. Clark, R.P. Tatom, S. Korposha, *Biosens. Bioelectron.* **75**, 222–231 (2016)
- H. Zhang, Z. Jia, X. Lv, *Curr. Appl. Phys.* **15**, 870–876 (2015)
- W. Qiong, L. Chen, L. Huang, J. Wang, J. Liu, H. Chao, H. Han, *Biosens. Bioelectron.* **74**, 16–23 (2015)
- B.I. Ipe, K. Yoosaf, K. George Thomas, *J. Am. Chem. Soc.* **128**, 1907–1913 (2006)
- X. Lv, L. Chen, H. Zhang, J. Mo, F. Zhong, C. Lv, J. Ma, Z. Jia, *Biosens. Bioelectron.* **39**, 329–333 (2013)
- H. Zhang, Z. Jia, X. Lv, J. Zhou, L. Chen, R. Liu, J. Ma, *Biosens. Bioelectron.* **44**, 89–94 (2013)
- G. Rong, J. Ryckman, R. Mernaugh, S.M. Weiss, *Appl. Phys. Lett.* **93**, 161109 (2008)
- F. Shi, Z. Jia, X. Lv, *Phys. Status Solidi A* 1–4 (2014)
- G. Gaur, D. Koktysh, S.M. Weiss, *Proc. SPIE* **8594**(3), 859408–11 (2013)
- Y-b Lee, S.H. Lee, S-y Park, C-j Park, K.-S. Lee, J. Kim, J. Joo, *Synth. Metals* **187**, 130–135 (2014)
- E. Cohen-Hoshen, G.W. Bryant, I. Pinkas, J. Sperling, I. Bar-Joseph, *Nano Lett.* **12**, 4260–4264 (2012)
- N.-Y. Kim, S.-H. YunHong, J.-W. Kong, N.S. Myoung, S.-Y. Yim, S. Jung, K. Lee, C.W. Tu, S.-J. Park, *RSC Adv.* **5**, 19624–19629 (2015)
- G. Gaur, D.S. Koktysh, S.M. Weiss, *Adv. Funct. Mater.* **23**, 3604 (2013)
- G. Frens, *Nat. Phys. Sci.* **241**, 20 (1973)
- J. Kimling, M. Maier, B. Okenve, V. Kotaidis, H. Ballot, A. Plech, *J. Phys. Chem. B* **110**, 15700 (2006)